New method for measuring diesel nozzle orifice inlet structures based on synchrotron X-ray tomography

Zhilong Li (李治龙)[1,2], **Zhijun Wu (吴志军)**[2*], **Ya Gao (高　雅)**[2], **Huifeng Gong (龚慧峰)**[2],
Weidi Huang (黄魏迪)[2], **Minjing Zhu (朱敏婧)**[2], and **Liguang Li (李理光)**[1]

[1]*School of Mechanical Engineering, Tongji University, Shanghai 200092, China*
[2]*School of Automotive Studies, Tongji University, Shanghai 200092, China*
*Corresponding author: zjwu@tongji.edu.cn

Spray behavior is regarded as one of the main factors influencing engine performances, fuel consumption and emissions for diesel engines. Under high injection pressure, diesel spray behaviors are extremely sensitive to the nozzle internal geometries, especially the geometric structures of orifice entrance. Based on the synchrotron radiation X-ray tomography technique, the 3D digital models of nozzle tips can be constructed. A new automatic method is presented to reveal the inlet structures according to these nozzle orifice models. The planes passing through the orifice axis are determined and used to cut the models, and then the corresponding cutting images are applied to measure the inlet chamfer radii around the orifice axis automatically. The orifices of a single-hole nozzle and an eight-hole nozzle are measured according to this method. The results show that this method can automatically measure the orifice inlet chamfer radii around the orifice axis with high precision. The obtained inlet chamfer radius shows the whole profile of the orifice entrance, which is a precise feedback for nozzle designing and manufacturing, and it also provides precise geometrical boundary conditions for the study of spray behaviors.

OCIS codes: 120.0120, 120.4290, 110.0110, 110.7440.
doi: 10.3788/COL201412.081201.

In modern diesel engines, the performance, efficiency, and pollutant emissions, are highly dependent on the quality of fuel sprays[1,2]. Therefore, diesel engines employ high injection pressures to achieve optimized breakup and atomization of liquid fuel sprays. Under such high injection pressures, the fuel flow inside the nozzle is extremely sensitive to its internal geometries, especially the orifice entrance geometric structures[3−6]. A sharp inlet corner can lead to flow recirculation and local cavitation, which under certain conditions can change the behaviors of the spray largely[7,8]. In order to improve the performance of diesel injection nozzles, the nozzle orifices are processed by hydro-grinding process after manufactured by electrical discharge machining (EDM)[9]. However, these processes are performed without closed-loop feedback controls, so the diameter, length, etc. of the manufactured orifices are hard to match the nominal dimensions closely. For the orifice entrances, there are even no nominal dimension requirements, as it is almost unavailable without destroying the nozzle until recent years. The lack of such entrance information hindered the researchers to compare and analyze the spray behaviors performed on different facilities.

In order to reveal the exact shape of the orifice entrance, a number of works have been done globally[10]. Traditionally the evaluation of the orifice entrance is based on the circle fitting of its inlet chamfer curve on a particular plane. This plane should pass through the axes of the nozzle and the testing orifice simultaneously. It is probably originated from the previously used destructive method of cutting the nozzle from the middle. Then the orifice inlet chamfer radius can be observed and measured directly on this cutting plane. In recent years

the nondestructive methods are broadly applied to measure the inlet chamfer radius, including the micro probing test method[11,12], silicone modeling method[13], and synchrotron radiation X-ray imaging methods[14,15]. However, on one hand these methods have their own problems. For example, the studies of probing method are still in the proof-of-concept stage. The shrinkage of silicone models during solidifying will cause unpredictable problems while measuring the inlet chamfer radius. The overlap of different orifices caused by the line-in-sight features of X-ray limits the usage of the synchrotron-based phase-contrast X-ray imaging approach on multi-hole nozzles. And the spatial resolution of industrial radiology and computed tomography (CT) still need further development. On the other hand, the orifice entrance is a three dimensional (3D) structure in reality, and the fuel flow inside the orifice is impacted by its whole internal structures. However, the current methods can only provide two inlet chamfer radii from one cutting plane for reference: the top and bottom chamfer radii. Some studies have confirmed that using the average inlet chamfer radius of single-hole nozzles based on several cutting planes can provide a better prediction of spray macro scope behaviors[16−18]. So only using the top and bottom chamfer radii to study the impacts of inlet structures on the fuel inner flow and spray atomization may lead to inaccurate or wrong results.

In this letter, a new method is presented to acquire precise structures of nozzle orifice entrance automatically. Based on the 3D digital models of nozzle tips, the orifice inlet chamfer radii around its axis are obtained. This geometrical information provides a precise feedback for nozzle designing and manufacturing, and can also provide

precise geometrical boundary conditions for the study of spray behaviors, and the modeling of fuel inner flow and primary atomization.

In order to construct the 3D digital models of nozzle tips, the synchrotron radiation X-ray was applied. It had excellent performance compared to the normal light source, including high intensity and high stability. In this study, the internal structures of diesel nozzle tips were constructed on the X-ray Imaging and Biomedical Applications Beam Line of the Shanghai Synchrotron Radiation Facility[19]. The experiment setup is sketched in Fig. 1(a). The diesel nozzle was held on the specimen rotating platform, and then X-ray penetrated its tip and irradiated on the scintillator crystal to convert the X-ray to visible light. A CCD camera was used to record the visible light. The pixel size of the camera was 7.4×7.4 (μm) corresponding to an actual spatial resolution of 3.7×3.7 (μm) with a 2× objective lens. The exposure time of a single frame was set to 8 s, and the photon energy of X-ray was tuned to 50 keV. Absorption images were taken every 0.25° with the nozzle rotating 180°, then totally 720 absorption images were captured during the CT scanning process.

During the reconstruction process, these absorption images are used to generate slices. However, the original slices might bare the defect of low signal to noise ratio. So they are converted to binary images and corresponding orifice images. By stacking these slices together, the digital models of orifices are reconstructed. The orifice digital models of an eight-hole nozzle and a single-hole nozzle are displayed in Fig. 1(b). Through these digital models, the internal structures of nozzles can be observed directly and clearly, but the measurement of such geometrical dimensions is not easy. As the 3D digital models obtained from the synchrotron X-ray CT are just numerical arrays stored in computers, the value at each point only represents whether it is inside or outside the orifice. So based on such a set of numbers, the acquisition of orifice geometrical dimensions needs further processing.
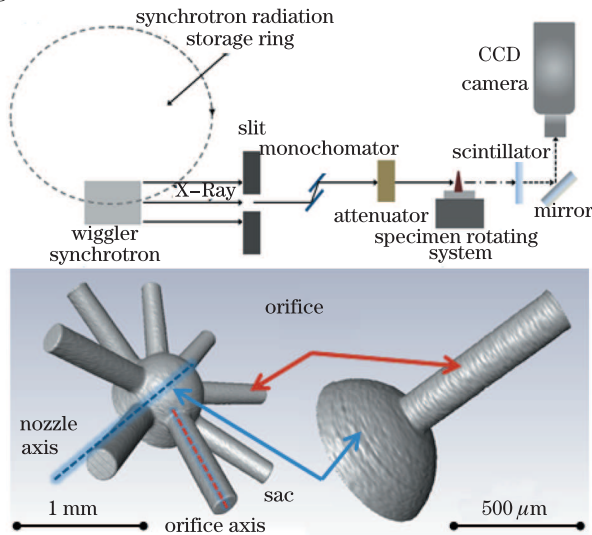

Fig. 1. (a) Procedure of recording the internal structures of nozzle tip by synchrotron radiation X-ray; (b) typical orifice 3D digital models of multi-hole (left) and single-hole (right) nozzle.

In order to evaluate orifice entrances, the planes across the orifice axis are all determined and applied to "cut" the orifices models from the middle. These planes are called "base planes" in this study. According to the cutting images between these base planes and the nozzle digital models, the curve of the entrance area can be exposed to calculate the best fitting circles. Based on this idea, the determination of all base planes and the acquistion of the optimized fitting circles are two key steps for the orifice inlet evaluation, and they will be discussed in more detail in the following sections.

According to the basic principle of conic sections[20], when a plane intersects with a cone, the cutting image would be a circle or an ellipse. The results only depend on whether this plane is perpendicular to the orifice axis or not. If so, the outcome image should finally be a circle, as shown in Fig. 2(a). This theory has laid a foundation for the determination of orifice axis. By selecting an arbitrary plane to intersect an orifice model, if the obtained cutting image is a circle, then the current plane is certainly perpendicular to the orifice axis. Otherwise, the cutting image of this plane should be an ellipse. According to the basic principles of geometry, the short axis of this ellipse should intersect with the orifice axis and perpendicular to it. Therefore, rotating this plane around the short axis is a reasonable method to find a specific angle to make this plane perpendicular to the orifice axis.

If the cutting image of a plane is an ellipse, its short axis will be fitted firstly according to the method of least square in this study. Then the original plane will rotate around this short axis with small angle steps. The cutting images at every angle are obtained and processed. So the determination of orifice axis has transformed to finding circles in these cutting images. Normally roundness is used for finding circles. The traditional methods usually compare fitting circles of the image (such as circumscribed or inscribed circles) with the nominal circle of the testing item, and then calculate roundness judgment parameters[21−23]. But in this study, no nominal circles can be provided to calculate the roundness parameter as the original plane is arbitrarily selected. However, according to the geometry principles, when the cutting plane is perpendicular to the orifice axis, the area of the current cutting image would be the minimum. So while rotating the cutting plane, the areas of each cutting images will be counted simultaneously. The corresponding value with minimum area on the abscissa should be the angle that the original arbitrary plane needs to rotate around the short axis, as shown in Fig. 2(b). After rotating, this plane should be perpendicular to the orifice axis. Meanwhile, the cutting image between this plane and the orifice model should be a circle, and the orifice axis should pass through the center of the circle. By fitting a straight line through the centers of the circles determined at different orifice positions, the orifice axis can be determined.

With the orifice axis being identified, the planes perpendicular to this axis can be rotated 90° around any diameter of the circle and become a base plane. Figure 2(c) shows a base plane of a single-hole nozzle. It is obvious that the obtained base plane has passed through the orifice axis. The corresponding cutting image is
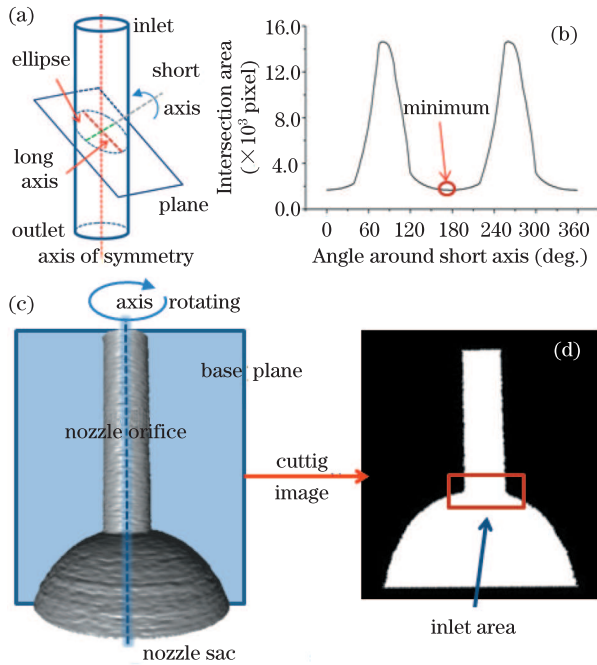
Fig. 2. (a) The sketch of cutting images between planes and cone; (b) the intersection image areas distribution of different rotating angles; (c) a base plane across a single-hole nozzle and (d) its corresponding cutting image.

displayed in Fig. 2(d), in which the square area with red line border is the concerning orifice entrance area. The curves there show the exact shape of the inlet, so in order to get a whole profile of the orifice entrance, the obtained base plane will rotate 180° around the orifice axis to cut the digital model by a tiny angle step, as demonstrated in Fig. 2(c). While the base plane is rotating, the cutting images at every angle will be stored for further processing.

Normally if the nozzle orifice inlet chamfer is gentler, the corresponding fitting circle will be larger. So the radius of this circle is usually used to evaluate the orifice inlet chamfer. However, currently there is no standard method for this inlet chamfer circle fitting. Traditionally this process is performed manually with the defects of low stability and high random errors. So in this study an automatic method was presented to calculate the inlet chamfer radius with higher accurate. This automatic circle fitting method is based on the Hough transform method[21]. The basic algorithm of this method is simple where a set of circles with different centers and radii are generated to "cover" the input curve. Then a series of circles which have covered at least one pixel of the inlet curve will be provided as outputs.

Figure 3(a) shows one cutting image between a base plane and the orifice model. In order to fit the circles, the area in the square with red dashed line border was extracted out and its edge was detected to find fitting circles by the Hough transform method, as shown in Fig. 3(b). Three fitting circles with top three covered pixel numbers of the inlet curve are displayed, and they are marked with $C1$, $C2$, and $C3$. Obviously $C3$ gives a wrong fitting of the inlet curve. The covered pixels are located on the orifice wall area near the entrance. However, this kind of wrong fitting circles usually covers only a few pixels, as shown in Fig. 3(f). The covered pixels

are much less than the circles fitting on the right location. So it is easy to get rid of these circles through the numbers of covered pixels. Circles $C1$ and $C2$ have fitted just the inlet area of this curve, but the radius of $C2$ is larger than $C1$. From Fig. 3(b) it can be found that $C1$ can match the inlet curve better than $C2$. The optimized result is amplified and displayed in Fig. 3(c).

Theoretically the circle covers the most pixel number should be chosen as the most fitting circle of the testing curve. However, in this study, under quite a few situations this principle has been found not suitable for the determination of the most fitting circle. The circle which covers the most pixels sometime is somewhat too large for the inlet curve. For example, from Figs. 3(d) and (e), it is obvious that the pixels covered by C_1 are most located in the bending area of the inlet, and these pixels are close to each other. Meanwhile, $C2$ has a bigger radius, and the pixels covered by $C2$ are a litter more than those covered by $C1$. But these pixels are distributed almost on orifice wall and orifice sac areas. They are separated into quite a few parts and far from each other. So it is hard to automatically determine the most fitting circle only based on the covered pixel number.

In order to overcome this limitation, a new algorithm was presented to determine the most fitting circle of inlet curves in this study. This algorithm takes into account the total covered pixel number (P_{num}) and the arc length in pixel (L_{arc}) of the testing circle from the start pixel (P_{start}) to the end pixel (P_{end}), as demonstrated in Eq. (1) and Fig. 3(e).

$$N = P_{\mathrm{num}} \times \frac{P_{\mathrm{num}}}{k \times L_{\mathrm{arc}}}, \tag{1}$$

where N is the optimized pixel number. The circles with the largest N will be selected as the most fitting circle. k is the correction factor, which can be set to appropriate value to obtain the optimized results. In this study it is set to 1, so according to Eq. (1), if the covered pixels are connected to each other, N will be equal to P_{num}, otherwise N will be smaller than P_{num}. Then according to this algorithm, the corresponding software was programed to automatically determine the most fitting circles. Figure 3(c) shows one optimized fitting result, from which it can be found that the result is quite reasonable for the
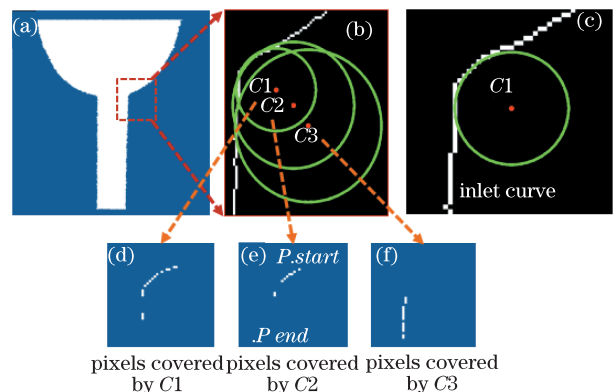

Fig. 3. The sketch of inlet chamfer radius calculation process (a) the cutting image; (b) the fitting circles of the testing orifice inlet chamfer curve; (c) the optimized fitting circle of the testing curve; (d)–(f) the overlapped pixels of the fitting circles and the testing curve.

testing curve.

As for each base plane, the corresponding cutting image contains two curves of the inlet chamfer, as shown in Fig. 3(a). These two curves are treated separately in this study. Then based on all these cutting images obtained by rotating the base plane, the whole profile of the inlet area can be established.

Two orifices are tested in this study. One orifice belongs to a single-hole nozzle and the other belongs to an eight-hole nozzle. The nominal outlet diameter of these two orifices is 160 μm, and after manufactured by EDM, they are both processed by hydro-grinding.

In order to improve the flow rate, the orifice axes of the single-hole nozzles are normally designed to be the same with the nozzle axes. So theoretically the inlet chamfer radius around the orifice axis should be the same in the single-hole nozzles. Figure 4 shows the orifice inlet chamfer radius result, in which the black line represents the radii around the orifice axis, and the red dashed line represents the average radius of this orifice, which is about 42.2 μm. Although the maximum radius is as large as 61.4 μm and the minimum radius is just 28.9 μm, it can still be found that the chamfer radii around the orifice axis are basically close to the average radius. These radii fluctuate only with a range of several micrometers. On the one hand, this fluctuation is a real reflection of the orifice inlet shape to a certain degree, as the processing cannot be absolutely uniform around the orifice axis. On the other hand, as the obtained cutting images are digital images, the discretization of digital pixels may cause a space oscillation, as the increase or decrease of one single pixel will cause a length variation of 3.7 μm. So this will certainly lead to a fluctuation in radius when performing circle fitting process. Nevertheless, it can be found that the amplitudes of radius fluctuation are almost around several micrometers, which means that the fluctuation in pixel is quite low, only one or two pixels. So if the spatial resolution is higher, the results should be much smoother.

From Fig. 4, it can also be found that the radii at the left side are basically smaller than the average radius, and the results at the right side are the other way round. This asymmetry is mainly caused by the offset between
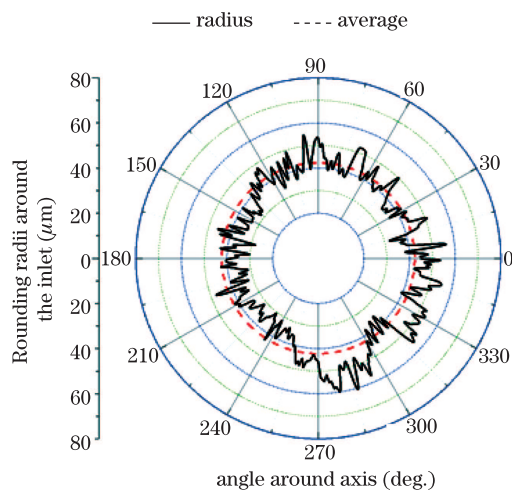

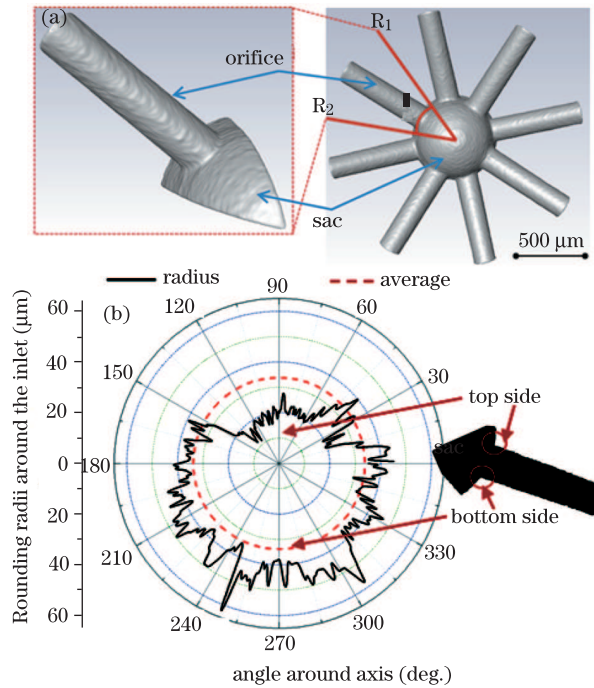Fig. 4. The inlet chamfer radii distribution around the orifice axis of a single-hole nozzle orifice.

Fig. 5. (a) The sketch of one orifice extracted from an eight-hole nozzle digital model; (b) the inlet chamfer radii distribution around the orifice axis of an eight-hole nozzle orifice.

the orifice axis and the nozzle axis, as the cutting image shows in Fig. 2(d). This kind of defect is quite common when processing single-hole nozzles. It has caused considerable difficulties when studying the impacts of the nozzle internal structures on spray behaviors.

For multi-hole nozzles, the orifices are processed separately. The inlet, outlet, and average diameters of the eight-hole nozzle are listed in Table 1. It can be found that the hole to hole dispersion is quite low. So one orifice is selected for analysis, and it was extracted from the whole digital model, as demonstrated in Fig. 5(a), to measure the inlet chamfer radii. Figure 5(b) shows the results, in which the red dashed line also represents the average radius of this orifice, and its magnitude is around 33.8 μm. Obviously the inlet chamfer radius asymmetry of this orifice is more notable, and its radius amplitudes fluctuation is higher than that of the single-hole nozzles. The maximum chamfer radius is about 64 μm, located at the bottom side. Meanwhile, the minimum chamfer radius is as small as 10 μm, located at the top side. This is because the orifices in multi-hole nozzles are drilled on the side wall of the nozzle sac without absolutely mutual perpendicular, and additionally the nozzle sac is a hemispherical shape processed in the nozzle tip. Thus the top side of the orifice inlet forms a sharp angle, and the bottom side forms an obtuse angle. The huge difference between them will affect the fuel flow inside the orifice significantly.

According to the measurement results, it can be found that the geometric structures of the orifice entrance are very complicated. Therefore, the traditional top and bottom chamfer radius measured in one plane which across the axes of the nozzle and the orifice cannot reflect the whole inlet entrance geometric structures. The whole orifice inlet chamfer radii measured in this study can

Table 1. The Inlet, Outlet, and Average Diameters of Each Orifice of the Eight-hole Nozzle

Diameters (μm)	Ori. 1	Ori. 2	Ori. 3	Ori.4	Ori. 5	Ori. 6	Ori. 7	Ori. 8
Inlet	169.5	168.0	167.7	169.9	170.0	168.6	170.1	167.5
Outlet	159.5	154.4	159.4	158.8	156.3	158.7	158.9	158.6
Average	165.0	164.3	165.3	166.3	167.0	165.1	165.5	164.2

be used to calculate the representative key parameters of the nozzle internal geometric structures, e.g. the average inlet chamfer radius, the maximum and the minimum radius, or the radius variance etc.. These key parameters can help researchers to study the influence of the nozzle internal geometric structures on spray behaviors and fuel flow rates.

Based on the synchrotron radiation X-ray tomography technology, the diesel nozzle 3D digital models are obtained, through which a new method is presented to measure the orifice inlet chamfer radius automatically. According to this method, the orifices of a single-hole nozzle and an eight-hole nozzle have been measured and analyzed. The following conclusions can be drawn from the results:

1) This orifice inlet chamfer radius automatic measurement method is feasible and reliable; the orifice inlet chamfer radii of a single-hole nozzle and an eight-hole nozzle have been measured with relative high precision.

2) The inlet chamfer circle fitting method presented is reliable according to the results, by which the inlet chamfer radii can be automatically fitted without manual intervention, and the random error can be limited to a very low level.

3) The traditional top and bottom chamfer radii cannot reflect a real condition of the orifice inlet geometry. They should be replaced by other key geometry parameters of orifice inlet structures, such as the average inlet chamfer radius, the maximum and minimum radius, or the radius variance.

4) The whole profile of the inlet chamfer radius distributed around the orifice axis provides new insights into the designing and manufacturing technology of nozzle orifices. They can also be used to describe the key internal geometry features of the orifice for the spray experiments and the simulation of fuel inner flow.

References

1. R. Payri, F. J. Salvador, J. Gimeno, and J. de la Morena, Appl. Therm. Eng. **29,** 2051 (2009).
2. S. Som, A. I. Ramirez, D. E. Longman, and S. K. Aggarwal, Fuel **90,** 1267 (2011).
3. T. R. Ohrn, D. W. Senser, and A. H. Lefebvre, Atomization Spray. **1,** 137 (1991).
4. R. Payri, F. J. Salvador, J. Gimeno, and L. D. Zapata, Fuel **87,** 1165 (2008).
5. Y. Wang, X. Liu, K. Im, W. Lee, J. Wang, K. Fezzaa, D. L. S. Hung, and J. R. Winkelman, Nat. Phys. **4,** 305 (2008).
6. R. Payri, F. J. Salvador, J. Gimeno, and L. D. Zapata, Fuel **87,** 1165 (2008).
7. W. Bergwerk, in *Proceedings of the Institution of Mechanical Engineers* **173,** 655 (1959).
8. C. Soteriou, R. Andrews, and M. Smith, SAE Paper **950080** (1995).
9. C. Diver, J. Atkinson, H. J. Helml, and L. Li, J. Mater. Process. Tech. **149,** 296 (2004).
10. A. L. Kastengren, F. Z. Tilocco, C. F. Powell, J. Manin, S. M. Pickett, R. Payri, and T. Bazyn, Atomization Spray. **22,** 1011 (2012).
11. C.-C. Kao and A. J. Shih, Meas. Sci. Technol. **18,** 3603 (2007).
12. E. Peiner, M. Balke, and L. Doering, Micro electron. Eng. **86,** 984 (2009).
13. V. Macian, V. Bermudez, R. Payri, and J. Gimeno, Exp. Tech. **27,** 39 (2003).
14. W.-K. Lee, K. Fezzaa, and J. Wang, Appl. Phys. Lett. **87,** 084105 (2005).
15. D. Lazaro, S. Legoupil, G. Blokkeel, and B. Jeanne, in *Proceedings of International Symposium on Digital industrial Radiology and Computed Tomography* (2007).
16. W. Huang, Z. Wu, H. Gong, Y. Gao, J. Deng, Z. Hu, and L. Li, SAE Paper 2013-01-1587 (2013).
17. Z. J. Wu, Z. L. Li, W. D. Huang, H. F. Gong, Y. Gao, J. Deng, and Z. J. Hu, Journal of Zhejiang University-Science A **13,** 182 (2012).
18. Y. Gao, W. Huang, Y. Gao, J. Deng, Z. Hu, Z. Wu, and L. Li, SAE Paper 2013-01-1611 (2013).
19. W. Chen, Y. Wang, H. Liu, B. Deng, Y. Yang, and T. Xiao, Chin. Opt. Lett. **12,** 023401 (2014).
20. Apollonius, *Treatise on Conic Sections* (Cambridge University Press, Cambridge,1896).
21. T.-H. Sun, Expert Syst. Appl. **36,** 3428 (2009).
22. B. Liu, P. Wang, Y. Zeng, and C. Sun, Chin. Opt. Lett. **8,** 666 (2010).
23. A. Al-Sharadqah and N. Chernov, Electron. J. Stat. **3,** 886 (2009).